CHIN. PHYS. LETT. Vol. 38, No. 7 (2021) 077302

Measurement of Superconductivity and Edge States in Topological Superconductor Candidate $TaSe_3$

Shuai Liu(刘帅)[1,2,3], Si-Min Nie(聂思敏)[4], Yan-Peng Qi(齐彦鹏)[1], Yan-Feng Guo(郭艳峰)[1], Hong-Tao Yuan(袁洪涛)[5], Le-Xian Yang(杨乐仙)[6,7], Yu-Lin Chen(陈宇林)[1,8,9], Mei-Xiao Wang(王美晓)[1,9*], and Zhong-Kai Liu(柳仲楷)[1,9*]

[1]*School of Physical Science and Technology, ShanghaiTech University, Shanghai 201210, China*
[2]*Shanghai Institute of Optics and Fine Mechanics, Chinese Academy of Sciences, Shanghai 201800, China*
[3]*University of Chinese Academy of Sciences, Beijing 100049, China*
[4]*Department of Materials Science and Engineering, Stanford University, Stanford, CA 94305, USA*
[5]*National Laboratory of Solid State Microstructures, College of Engineering and Applied Sciences, and Collaborative Innovation Center of Advanced Microstructures, Nanjing University, Nanjing 210093, China*
[6]*State Key Laboratory of Low Dimensional Quantum Physics, Department of Physics, Tsinghua University, Beijing 100084, China*
[7]*Frontier Science Center for Quantum Information, Beijing 100084, China*
[8]*Department of Physics, University of Oxford, Oxford, OX1 3PU, UK*
[9]*ShanghaiTech Laboratory for Topological Physics, Shanghai 201210, China*

(Received 29 March 2021; accepted 12 May 2021; published online 3 July 2021)

Topological superconductors (TSCs) have been widely investigated in recent years due to their novel physics and ability to host Majorana fermions (MFs) which are key to topological quantum computation. Despite the great interest, only a few compounds have been proposed as candidates of intrinsic TSCs, such as iron-based superconductor $FeSe_{0.55}Te_{0.45}$ and 2M-WS_2. Among them, quasi-one-dimensional superconductor $TaSe_3$ possesses fascinating properties such as its simple stoichiometry, layered nature and chemical stability. Here, using scanning tunneling microscope/spectroscopy (STM/STS), we systematically investigate the topography and electronic structure of $TaSe_3$. Our STM/STS measurement reveals large atomically flat, defect-free surfaces suitable for the search of MF; electronic density of states consistent with our angle-resolved photoemission result and band-structure calculations, and a uniform superconducting gap with a typical size of ∼0.25 meV. Remarkably, additional edge states are observed in the vicinity of the terrace edge, suggesting they may have a topological origin. Our result proves the coexistence of superconductivity and topological electronic structure in $TaSe_3$, making it an intriguing platform to investigate topological superconductivity.

DOI: 10.1088/0256-307X/38/7/077302

Over the past few years, the search and investigation of topological superconductors (TSCs) have attracted great interest for condensed matter physicists. TSCs are a new type of superconductor with a topologically non-trivial electronic structure that leads to the emergence of Majorana fermions (MFs). MFs are a kind of particle that is identical to its own anti-particle. It obeys the non-Abelian statistics and could be used as topological qubits,[1] the base unit for topological quantum computation. Several material systems have been proposed to be TSCs, including the odd parity p-wave superconductors,[2] heterostructures with interfaces between a superconductor and topological insulator/semimetal, or a semiconductor with strong spin-orbit interaction.[3−12] The MF and Majorana bound states (MBSs) have been observed in interfaces between InAs/InSb nanowires/superconductors, and (Bi, Sb)$_2$Te$_3$/superconductors.[7,9,10,13]

Another route to achieve TSC is through materials that host both superconductivity and spin-polarized topological electronic states, thus avoiding the difficulty in the construction of complicated heterostructures with a perfect interface. Following this route, a large number of materials have been proposed and examined, including iron-based superconductors $FeTe_{0.55}Se_{0.45}$,[14−16] Li(Fe,Co)As,[17] $(Li_{0.84}Fe_{0.16})$OHFeSe,[18] 2M-WS_2,[19−21] and β-Bi_2Pd.[22−24] In these materials systems, characteristic topological surface states (TSSs) and/or signatures of MBSs have been observed by angle-resolved photoemission spectroscopy (ARPES) and scanning tun-

Supported by the National Key R&D Program of China (Grant No. 2017YFA0305400), the Shanghai Technology Innovation Action Plan 2020-Integrated Circuit Technology Support Program (Grant No. 20DZ1100605), the National Natural Science Foundation of China (Grant Nos. 52072168, 21733001, 51861145201, U1932217, and 11974246), the National Key Basic Research Program of China (Grant No. 2018YFA0306200), and the Science and Technology Commission of Shanghai Municipality (Grant No. 19JC1413900).
*Corresponding authors. Email: wangmx@shanghaitech.edu.cn; liuzhk@shanghaitech.edu.cn
© 2021 Chinese Physical Society and IOP Publishing Ltd

neling microscope/spectroscopy (STM/STS) experiments. The currently available materials are not ideal, however, due to high defect level ($FeTe_{0.55}Se_{0.45}$), being in the metastable state (2M-WS_2) or being difficult to exfoliate (iron-based superconductors and β-Bi_2Pd).

Recently, a new member of the TSC material candidate, i.e., transition-metal trichalcogenide $TaSe_3$, has been proposed and investigated.[25−28] Compared with the materials mentioned above, $TaSe_3$ is stoichiometric, exfoliable and stable in the ambient environment and possesses TSSs crossing the Fermi level. $TaSe_3$ also holds intriguing physical properties such as large non-saturating magnetoresistance,[27,29] a topological phase transition under external strain and signatures of multiple mobile excitons.[28] Moreover, theorists proposed a quantum spin Hall insulator (QSHI) phase in the monolayer of $TaSe_3$ and the helical topological edge state is expected to form a one-dimensional (1D) TSC.[26,28,30] These intriguing properties make $TaSe_3$ an important platform to study the interplay between topology and superconductivity.

In our previous ARPES investigation on $TaSe_3$,[26] we systematically investigated its electronic structure and identified the non-trivial TSSs. In this Letter, we report the STM investigations of $TaSe_3$ in aspects of surface topography, electronic structure and superconductivity of $TaSe_3$. Our STM/STS measurement reveals large terraces of $TaSe_3$ with tiny amount of impurities/defects on the cleavage surface, suitable for the search of the MBSs; semimetal-type electronic density of state (DOS) with reduced DOS at the Fermi energy E_F, consistent with our angle-resolved photoemission result and band structure calculations, and a uniform superconducting gap with typical sizes of ∼0.25 meV. Moreover, we observed additional edge states located in the vicinity of the terrace step edge, showing consistency with the edge-projected calculation of the local DOS of the $TaSe_3$ monolayer and suggesting they may have a topological origin. Our STM investigation provides critical information on $TaSe_3$ and hints it hosts non-trivial topological superconductivity in both bulk form and the monolayer limit.

STM/STS measurements were carried out in a commercial Joule–Thomson (JT) STM system combined with a sample preparation chamber supplied by Unisoku cooperation, Japan. $TaSe_3$ single crystals were cleaved in an ultrahigh vacuum at room temperature. After cleavage, samples were transferred *in situ* to the STM sample stage connected to a cryogenic stage kept at 77.8 K (by liquid nitrogen), 5.2 K (by liquid Helium) and 1.2 K (by JT cooling) for STM/STS experiments. PtIr tips were used for both imaging and tunneling spectroscopy, which were all carefully calibrated through the surface states of silver islands grown on Si (111). Lock-in technique was employed to obtain dI/dV curves with high energy resolution and low noise.

The full-potential linearized augmented plane-wave method implemented in the WIEN2K simulation package[31] was employed to perform the first-principles calculations. The modified Becke–Johnson exchange potential was used to obtain accurate band structures.[32] A $21\times6\times1$ k-point grid was used in the self-consistent calculations with the consideration of spin-orbit coupling. The radii of the muffin-tin sphere R_{MT} were 2.5 bohr and 2.38 bohr for Ta and Se, respectively. The truncation of the modulus of the reciprocal lattice vector K_{max} was set to $R_{MT}K_{max} = 7$. To explore the edge states, maximally localized Wannier functions for the d orbitals of Ta and p orbitals of Se were constructed.[33]

The characterization of the $TaSe_3$ samples we measured could be found in Ref. [26]. $TaSe_3$ has a monoclinic structure with space group $P2_1/m$ (No. 11).[34] It is crystallized by two inequivalent types of Ta atomic chains (green ball) which are in parallel arrangement along the b direction. Each Ta atom within a chain is surrounded by three Se atoms (blue balls) forming a quasi-1D crystal structure, as shown in Figs. 1(a) and 1(b). Besides the chain-like structure, $TaSe_3$ also possesses a layered crystalline structure due to the weak bonding of Se–Se atoms between two Se saturated $(10\bar{1})$ surfaces. Therefore, the $TaSe_3$ single crystal can be easily cleaved along its $[10\bar{1}]$ direction to obtain a large cleavage surface. Figure 1(c) (upper panel) shows the surface topographic image of the cleavage plane, where large flat terraces with sharp and straight step edges can be observed. To better reveal the atomically flat surface, the lower panel of Fig. 1(c) presents the line-profile of height across the step (the position of the measurement is indicated in the upper panel). The step height is 0.82 nm, very close to the lattice constant of the $TaSe_3$ single crystal in the $[10\bar{1}]$ direction. The saw-toothed feature on the terrace region in the line-profile in the lower panel of Fig. 1(c) reflects the parallel arrangement of the Ta atomic chains, as can also be observed in the topography. Cruising the STM tip onto the flat area of the cleavage surface, clear chain-like structure with a lattice constant of 1.25 nm (space between two chains) and 0.355 nm (space between two Ta atoms along a chain) are obtained from the atomically resolved image and the corresponding line-profile in Fig. 1(d), both of which are consistent with the lattice structure of the $(10\bar{1})$ surface. We also noticed that very few defects could be identified as we scan over the flat terrace. Our STM topographic images in Figs. 1(c) and 1(d) prove that the cleavage surface of our $TaSe_3$ sample shows extremely high quality, which guarantees reliable surface-sensitive measurements (such as STM and ARPES) as well as a clean platform for the

search of the MF/MBS.

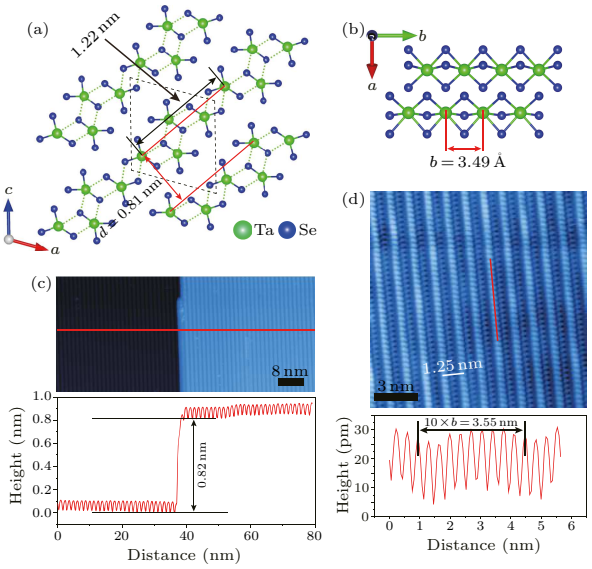

Fig. 1. [(a), (b)] Ball and stick model showing the crystal structure of $TaSe_3$: (a) ac plane with one surface unit cell labelled by the black dotted line and (b) ab plane. Green balls represent Ta atoms and blue balls represent Se atoms. The red and black arrow in (a) indicates the distance between two adjacent $(10\bar{1})$ cleavage planes and two identical chains, respectively. (c) Upper panel: large scale STM image in 80 nm × 35 nm showing the atomically flat surface of $TaSe_3$ with a sharp and straight step (I_s = 250 pA, U_s = 400 mV). Lower panel: line-profile along the red line given in the upper panel revealing the step height. (d) Upper panel: STM atomic resolution image of the cleavage plane showing a clear chain-like surface structure (15 nm × 15 nm, I_s = 200 pA, U_s = 15 mV). Lower panel: line-profile revealing the lattice constant along a Ta atomic chain.

We investigated the electronic structure of $TaSe_3$ by the STS. Figure 2(a) shows a series of dI/dV spectra across multiple atomic chains; it can be clearly seen from the figure that there are two obvious peaks below the E_F at ∼−0.15 eV and ∼−0.4 eV, respectively. Moreover, the DOS of the two peaks fluctuates with the atomic chains. We obtained the spatially averaged STS from these dI/dV spectra, as shown in Fig. 2(b). The positions of peaks are in agreement with the momentum-integrated energy distribution curve (EDC) from the ARPES measurement [Fig. 2(c)], as well as the calculated DOS [Fig. 2(d)]. By aligning the first peak below E_F [the black arrow in Fig. 2(b)], one can find that there is an overall agreement but the ∼48/105 meV shift in the E_F between dI/dV and EDC/calculated DOS, respectively. The energy shift between dI/dV and EDC may come from the mesoscopic spatial inhomogeneity together with the rather localized probing size in the STM experiment. The energy difference between the experiment and calculation may come from the imperfection of the sample and the details of the DFT calculation. In addition, we have noted that a dI/dV shape near E_F is not well reflected in the calculated DOS, which is attributed to the fact that the calculated DOS does not include the TSSs near E_F.

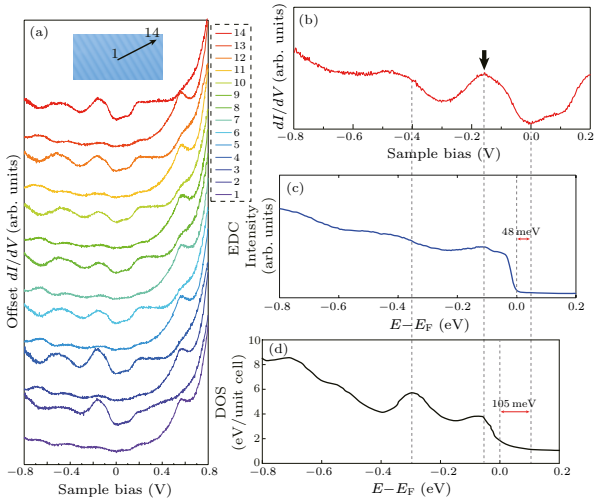

Fig. 2. (a) A series of dI/dV spectra along the defined black line in the inset panel with sample bias from −0.8 V to +0.8 V. (b) Averaged dI/dV spectrum of $TaSe_3$. (c) Integrated energy distribution curve (EDC) from the ARPES map measured using photons of $h\nu$ = 30 eV at 10 K. (d) Calculated total density of states (DOS) of $TaSe_3$, data extracted from Ref. [25].

Figure 3(a) shows a topographic image of a 30 nm × 30 nm area where superconducting gaps are closely inspected. We randomly chose six different locations within this area to measure their dI/dV curves near E_F. As an example, the STS obtained at 1.2 K at point A is plotted in the gray curve in Fig. 3(b), where a pronounced gapped feature can be found at E_F. To demonstrate that it is indeed a superconducting gap, we raise the sample temperature to 5.2 K beyond its T_c. We find that the gap at the E_F is vanished as expected, as shown by the blue curve in Fig. 3(b). Furthermore, we employ the Dynes equation,[35] which abides Bardeen–Cooper–Schrieffer (BCS) theory to fit the curve obtained at 1.2 K. The fitting result is plotted in the red solid curve and superimposed directly onto the experimental result for comparison. One can see that the gap feature can be well depicted by the Dynes equation. Moreover, the fitted parameter of the Dynes equation $\Delta_s = 0.275$ meV and $T_c \approx \frac{2\Delta_s}{3.53k_B} = 1.81$ K based on the BCS theory, are in agreement with the T_c of $TaSe_3$ reported by previous works,[36,37] revealing an s-wave superconductivity behavior in $TaSe_3$.

Furthermore, we studied the homogeneity of the superconducting gaps. In Fig. 3(c) we stack plot all the dI/dV curves measured at the other five spots measured at 1.2 K from Fig. 3(a), which qualitatively shows uniform superconducting gaps. By fitting all these curves using the Dynes equation, we obtain the Δ_s values and list them in Table 1, from which one

can conclude that the superconductivity is homogenous. We take 0.25 meV (the average value of superconducting gaps listed in Table 1) as a typical value of the superconducting gap.

Table 1. The value of superconducting gaps of $TaSe_3$ at different locations.

Number of points	1	2	3	4	5	Average
Δ_s (meV)	0.26	0.24	0.25	0.23	0.28	0.25

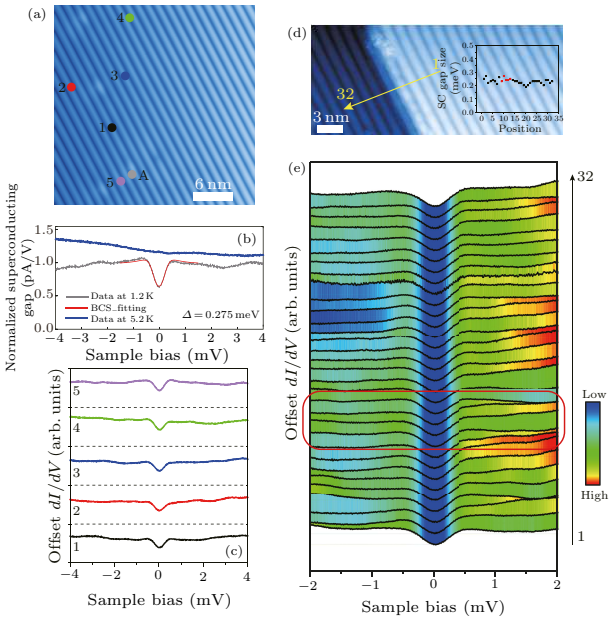

Fig. 3. (a) Topographic image in 30 nm × 30 nm of the cleavage plane giving six different positions for superconducting gap measurements (I_s = 200 pA, U_s = 12 mV). (b) Single-point STM dI/dV curve near Fermi energy measured at 1.2 K showing the superconducting gap of $TaSe_3$ (gray line) superimposed with the Bardeen–Cooper–Schrieffer (BCS) theory fitting curve (red line). The dI/dV curve measured at 5.2 K within the same energy range is plotted as a comparison (blue line). (c) Offset dI/dV curves measured at 1.2 K at five different points given in (a). (d) Positions of the 32 points where superconducting gaps are measured indicated by the yellow arrow on the STM topographic image in 30 nm × 13 nm at 1.2 K (I_s = 200 pA, U_s = 25 mV). Inset panel: position dependence of superconducting gap size Δ_s fitted by the Dynes equation. (e) Stacking plot of all the superconducting gaps taken on the 32 points.

The uniformity of the superconducting gap at 1.2 K is further studied by a line cut across the terrace step edge [Fig. 3(d)]. Figure 3(e) shows the stack plot of a 32-point dI/dV line cut perpendicular to a step edge [Fig. 3(d)], where we find there is no apparent change near the step edge (the curves in the red rounded rectangle represent curves measured at the point near the step edge). To quantitatively prove this, we fit all these curves to obtain the size of gap Δ_s and plot the fitting result as a function of position, as shown in the inset panel in Fig. 3(d) (the red points represent the position near the step). The gap size slightly fluctuates with changing the measuring point but shows no relevance to the position of the step.

Here, we would like to note that the dI/dV spectra at E_F shown in Fig. 3 never reaches zero, indicating that there are some non-superconducting normal states at E_F. We think these results are simply the consequence of the finite measuring temperature 1.2 K, which is over 60% of the T_c. We believe a more pronounced superconducting gap with sharper coherence peaks and zero-conductance at E_F should be obtained at a lower measurement temperature.

Lastly, we report the observation of the edge states in $TaSe_3$. In Fig. 4(a), we show a large-scale STM topographic image with a clear stripe-like structure and terrace steps. Figure 4(b) shows a series of consecutive dI/dV curves along a line (with 53 points) across two steps [black line in Fig. 4(a)]. The electronic states at points far away from the step are plotted by the blue lines and are almost identical at all terraces. In contrast, we find that the curves near the step edge (red line) are quite different: the intensity at sample bias lower than ∼−100 meV has much higher intensity revealing the existence of edge states in $TaSe_3$. We select one typical curve measured at point A far away from the edge and a curve measured at point B on the upper terrace close to the edge and plot them together in Fig. 4(c). Through the comparison of these two curves, we can hardly tell any difference within the bias range +0.4 V to −0.1 V so that we can rule out the possibility of external condition change (e.g. modified status of the STM tip). To better visualize the edge states, we draw an intensity map using the same data in Fig. 4(b) with the distance shown in Fig. 4(d)(iii). Apparently, we find that the period in the dI/dV intensity comes from the chain structure and the edge states at negative bias near the step edges could be clearly distinguished (labeled by the red color). In addition, a decay length of 0.45 nm is fitted by the exponential function, which is similar to the decay length of topological edge states observed in the QSHI bismuthene film grown on SiC,[38] and smaller than the decay length about 1.6 nm of the terrace edge state in $ZrTe_5$.[39] The small decay length indicates the observed edge states distribute closely along the step edge and extend laterally in a scale smaller than a primitive cell (the distance between two chains is 1.25 nm).

The additional electronic states observed in the step edge show great resemblance to the edge state found in WTe_2, $HfTe_5$, and $ZrTe_5$.[39–44] Given that the $TaSe_3$ is predicted to be a QSHI in its monolayer limit,[26,28] it is highly likely that the edge state of $TaSe_3$ possesses a topologically non-trivial origin, similar to the WTe_2 case. To justify this point, we carried the first-principle calculation on the band structure along the Y–Γ–Y direction of the monolayer $TaSe_3$ [Fig. 4(e)] and edge-projected local DOS to the Ta–Se

chain termination [along $\bar{Y}$–$\bar{\Gamma}$–$\bar{Y}$, Fig. 4(f)]. In addition to the broadening of the monolayer dispersion [Fig. 4(e)] due to the edge-projection, several sharp dispersions could be found near E_F [we shift the E_F of the calculation by 105 meV for comparison in Fig. 4(f), similar to Fig. 2(d)] and below, and identified as the topological edge states in the QSHI phase [Fig. 4(f)]. To show that the calculation results of monolayer $TaSe_3$ can be compared with the case of a surface step of bulk, we also calculated the interlayer binding energy of $TaSe_3$. The calculated binding energy is 19.156 meV/Å^2, which is much smaller comparing to the interlayer coupling of Bi_2Se_3 (27.6 meV/Å^2) and Bi (111) (40.1 meV/Å^2) bilayer and slightly higher than $ZrTe_5$ (12.5 meV/Å^2),[45] indicating a week interlayer coupling nature in $TaSe_3$. Given the observed topological edge states on the step edge of $ZrTe_5$,[39,41] and the overall agreement between the energy position of the calculated edge states and measured DOS of edge states, it is very likely that the physics is similar in $TaSe_3$ that the edge state found on the step edge reflects the monolayer property and has a non-trivial topological origin.

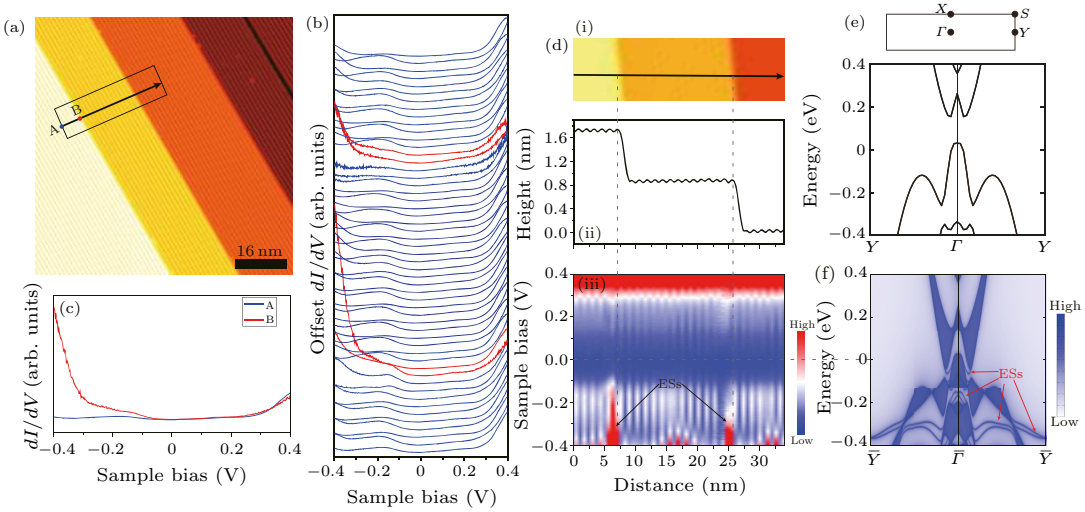

Fig. 4. (a) Large-scale STM topographic image on $TaSe_3$ with several sharp steps measured at 77 K (80 nm × 80 nm, I_s = 250 pA, U_s = 0.4 V). (b) Stacking STS curves along a defined line (53 points) drawn in (a) across two steps. (c) Two selected dI/dV curves at measuring points far from the step (labeled as A) and near the step (labeled as B) shown in (a), respectively. (d) Color mapping of the dI/dV curves as a function of distance (iii) and the plot of its corresponding line-profile (ii) along the defined line given in (i). (e) Brillouin zone of monolayer $TaSe_3$ (upper panel) and calculated band structure along the Y–Γ–Y direction of monolayer $TaSe_3$. (f) The calculated edge-projected local DOS along the $\bar{Y}$–$\bar{\Gamma}$–$\bar{Y}$ direction. The topological edge states (ESs) are labeled. The E_F of the calculation is shifted by 105 meV for comparison with (d)(iii), similar to Fig. 2(d), as indicated by the dotted line.

The high sample quality, defect-free surface, uniform superconductivity and edge states make $TaSe_3$ a unique system for the search of MBS. So far, most works addressing the MBS are achieved by the observation of characteristic zero modes on a vortex core in TSCs using STM/STS.[3,4,7,46,47] For detecting true MBSs in a vortex, a nice quality of the samples with large flat surface free of impurities and defects is firstly required. On the one hand, the vortices tend to be pinned by impurities and defects, which would also contribute to a sharp peak at E_F.[48] On the other hand, the area of the surface should be large enough to ensure the safe distance between two vortices to protect them from annihilating,[13] which becomes a challenging task, especially for the epitaxial thin films. Moreover, the homogeneity of superconductivity of a TSC is essential because it will ensure the uniform distribution of the vortices and their core states for the reliable detection of MBSs. In addition, the coexistence of topological edge states and superconductivity may form a new type of 1D TSC. The helical edge state in QSHI in coexistence with the superconductivity may lead to the formation of the MBS near defects in the step edge, similar to the case of the InAs/InSb nanowire on superconductors.

In summary, our systematic STM/STS measurement on the TSC candidate $TaSe_3$ reveals large atomically flat defect-free surfaces suitable for the search of MF, the electronic DOS consistent with our angle resolved photoemission result and band structure calculations, and highly homogeneous superconducting gaps independent of the measuring points on the flat surface or near step edges with typical sizes ∼0.25 meV, which fit well with the BCS theory and reveal the conventional s-wave superconducting behavior in $TaSe_3$. Remarkably, additional edge states are observed in the vicinity of the terrace edge, suggesting they may have a topological origin. Our result proves the coexistence of superconductivity and topological electronic structure in $TaSe_3$, making it an intriguing

platform to investigate topological superconductivity.

References

[1] Nayak C *et al.* 2008 *Rev. Mod. Phys.* **80** 1083
[2] Das S S, Nayak C and Tewari S 2006 *Phys. Rev. B* **73** 220502
[3] Das A *et al.* 2012 *Nat. Phys.* **8** 887
[4] Deng M T *et al.* 2012 *Nano Lett.* **12** 6414
[5] Mourik V *et al.* 2012 *Science* **336** 1003
[6] Wang M X *et al.* 2012 *Science* **336** 52
[7] Finck A D K *et al.* 2013 *Phys. Rev. Lett.* **110** 126406
[8] Nadj-Perge S *et al.* 2014 *Science* **346** 602
[9] Albrecht S M *et al.* 2016 *Nature* **531** 206
[10] Deng M T *et al.* 2016 *Science* **354** 1557
[11] Zheng H and Jia J F 2019 *Chin. Phys. B* **28** 67403
[12] Guo B *et al.* 2020 *Chin. Phys. B* **29** 097403
[13] Sun H H *et al.* 2016 *Phys. Rev. Lett.* **116** 257003
[14] Wang D F *et al.* 2018 *Science* **362** 333
[15] Zhang P *et al.* 2018 *Science* **360** 182
[16] Zhu S Y *et al.* 2020 *Science* **367** 189
[17] Zhang P *et al.* 2019 *Nat. Phys.* **15** 41
[18] Liu Q *et al.* 2018 *Phys. Rev. X* **8** 041056
[19] Yuan Y H *et al.* 2019 *Nat. Phys.* **15** 1046
[20] Fang Y Q *et al.* 2019 *Adv. Mater.* **31** 1901942
[21] Li Y W *et al.* 2021 *Nat. Commun.* **12** 2874
[22] Guan J Y *et al.* 2019 *Sci. Bull.* **64** 1215
[23] Lv Y F *et al.* 2017 *Sci. Bull.* **62** 852
[24] Li Y F *et al.* 2019 *Science* **366** 238
[25] Nie S M *et al.* 2018 *Phys. Rev. B* **98** 125143
[26] Chen C *et al.* 2020 *Matter* **3** 2055
[27] Xia W *et al.* 2020 *Phys. Rev. B* **101** 155117
[28] Ángel S G J and Canadell E 2020 *2D Mater.* **7** 025038
[29] Zhang Y *et al.* 2020 *AIP Adv.* **10** 095314
[30] Hart S *et al.* 2014 *Nat. Phys.* **10** 638
[31] Blaha P *et al.* 2001 *WIEN2K: An Augmented Plane Wave Plus Local Orbitals Program for Calculating Crystal Properties* (TU Vienna, Vienna)
[32] Tran F and Blaha P 2009 *Phys. Rev. Lett.* **102** 226401
[33] Marzari N *et al.* 2012 *Rev. Mod. Phys.* **84** 1419
[34] Yamaya K and Oomi G 1982 *J. Phys. Soc. Jpn.* **51** 3512
[35] Dynes R C, Narayanamurti V and Garno J P 1978 *Phys. Rev. Lett.* **41** 1509
[36] Sambongi T *et al.* 1977 *J. Phys. Soc. Jpn.* **42** 1421
[37] Tritt T M, Stillwell E P and Skove M J 1986 *Phys. Rev. B* **34** 6799
[38] Reis F *et al.* 2017 *Science* **357** 287
[39] Wu R *et al.* 2016 *Phys. Rev. X* **6** 021017
[40] Tang S J *et al.* 2017 *Nat. Phys.* **13** 683
[41] Li X B *et al.* 2016 *Phys. Rev. Lett.* **116** 176803
[42] Liu S *et al.* 2018 *APL Mater.* **6** 121111
[43] Peng L *et al.* 2017 *Nat. Commun.* **8** 659
[44] Liu R Z *et al.* 2019 *Chin. Phys. Lett.* **36** 117301
[45] Weng H M, Dai X and Fang Z 2014 *Phys. Rev. X* **4** 011002
[46] Manna S *et al.* 2020 *Proc. Natl. Acad. Sci.* **117** 8775
[47] Feldman B E *et al.* 2017 *Nat. Phys.* **13** 286
[48] Yin J X *et al.* 2015 *Nat. Phys.* **11** 543